Marta Alvarez Puig

Porous alumina-based electrochemical biosensor to support the early diagnosis of lung cancer

Final Degree Project

Supervised by Dr. Beatriz Prieto Simón
Co-supervised by Deepanshu Verma

Degree in Biomedical Engineering

UNIVERSITAT ROVIRA I VIRGILI

Tarragona
2023

ACKNOWLEDGEMENTS

First of all, I would like to thank Dr. Beatriz Prieto Simón for giving me the opportunity to do this work, because from the first day we talked and I told her what I would like to do, just with my preferences on how to approach it, she put full trust in me.

At the same time, I would like to thank Deepanshu Verma, who has supervised my work and helped and guided me day after day in the lab. Thank you for the help you have given me, for being in line with what I needed and for passing on your knowledge in this field.

To thank the lab group, who made my stay enjoyable and helped me when I needed it.

Finally, I would like to thank my family and my flatmates for their constant love and support during this time.

I would also like to remember and thank the person who inspired me to do this work, my grandfather.

INDEX

1 Introduction

1.1 Project

Despite significant progress in chemotherapy, radiotherapy, and surgical interventions, cancer continues to be a major contributor to global mortality. Among various types of cancer, lung cancer stands out as the leading cause of cancer-related deaths worldwide, with a discouraging five-year survival rate of approximately 16% when diagnosed at an early stage. An essential aspect of lung cancer classification involves examining the microscopic appearance and size of cancer cells. Based on these characteristics, lung cancer can be broadly categorized into two classes: non-small cell cancer and small cell cancer [1][2].

Small-cell lung cancer accounts for about 15% of the total. This is a type of cancer that affects small cells as seen under the microscope. This cancer is more aggressive than non-microcytic type and progresses more rapidly [3].

Non-microcytic lung cancer, also called non-small cell lung cancer, is the most common type of lung cancer, comprising 80% to 85% of all lung cancers. Subtypes of this cancer include adenocarcinoma, a non-squamous cell cancer, which is the most frequent, squamous cell carcinoma, and finally large cell carcinoma, which is the least frequent of the three subtypes.

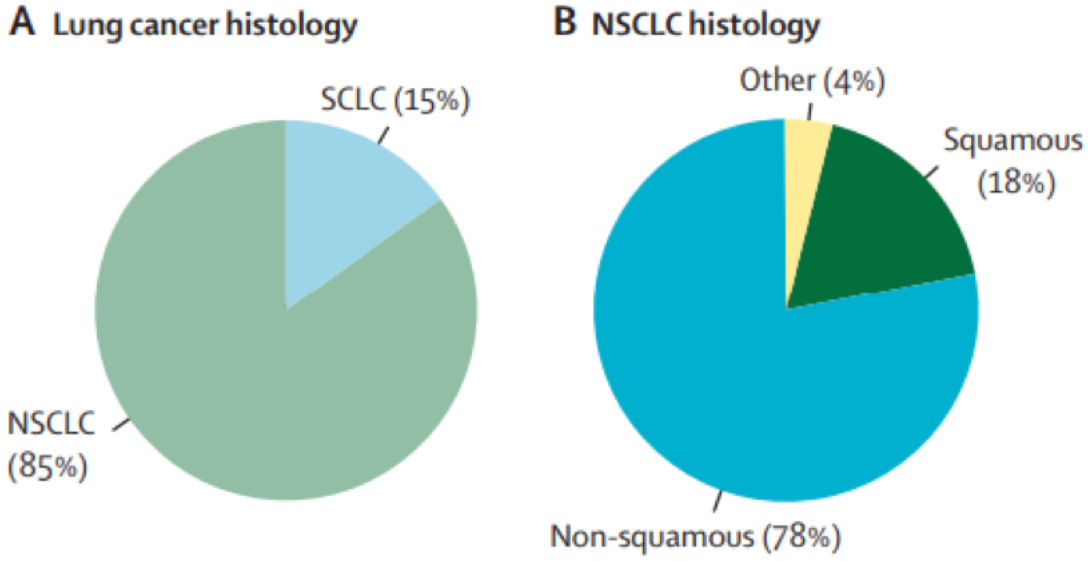

Figure 1. Classes of lung cancer based on the size adapted from [1].

The relatively low 5-year survival rate of a lung cancer patient, the high prevalence and mortality of two subtypes of non-small cell lung cancer, namely adenocarcinoma and squamous cell carcinoma, and the resistance that patients develop throughout the course of the disease to therapies, create a need for research into the development of tools for early stage diagnosis.

Extensive research efforts have dedicated considerable attention to exploring the role of miRNAs in cancer studies. MiRNAs, which are small RNA molecules consisting of around 21 to 24 nucleotides, have emerged as significant regulators of gene expression. Their potential as biomarkers for various cancer subtypes lies in their ability to exhibit

distinct expression patterns that correlate with clinicopathological parameters. Additionally, miRNAs offer promise in identifying treatment resistance, expanding their utility in cancer management and prognosis.

One intriguing aspect of miRNAs is their stability in bodily fluids, where they are enclosed within vesicles. This stability enables non-invasive imaging techniques such as MRI or CT to detect and analyze these miRNAs. Investigating their role in cancer development has revealed specific miRNAs, such as miR-21, the miR-17-92 cluster, and miR-221/222, functioning as oncogenes that drive tumor progression. Conversely, certain miRNA families, including let-7, miR-34, and miR-200, act as tumor suppressors. Recent breakthroughs have shed light on key miRNAs involved in cancer diagnosis and treatment by examining circulating tumor cells and microvesicle exudates like exosomes.

In summary, the extensive exploration of miRNAs and their implications in cancer research has provided invaluable insights into diagnosing cancer, predicting prognosis, and devising therapeutic strategies. Analyzing circulating biomarkers and exosomal miRNAs has proven particularly fruitful in unravelling the intricate mechanisms underlying cancer development and progression.

miR-155 was identified as the first miRNA with a potential oncogenic role. Another miRNA that plays a similar role in lung cancer is miR-21, which is overexpressed and acts by inhibiting negative regulators involved in cell death and PTENs, resulting in increased cell proliferation.

In non-small cell lung cancer, the family of miRNAs known as miR-200 has been found to be overexpressed [4].

Detecting these biomarkers can aid cancer diagnosis at an early stage, which is crucial because it brings several benefits:

1. More Treatment Options: Diagnosing cancer early means more treatment choices. Less invasive and more effective treatments are often available at the early stages. When cancer is advanced, treatment options become limited and less successful.
2. Better Survival Rates: Detecting cancer early increases the chances of successful treatment and higher survival rates. When cancer is diagnosed early, it is usually still localised in one place and easier to cure. This leads to better long-term outcomes for patients.
3. Personalized Treatment: Early detection helps doctors make personalized treatment decisions. Biomarkers provide important information about the specific characteristics of the cancer. This allows doctors to tailor treatment plans to each patient's unique situation, leading to better results.
4. Reduced Side Effects: Early detection may help avoid aggressive treatments that can have severe side effects. By finding cancer early, less invasive and less harmful treatment options can be used. This improves the patient's quality of life during and after treatment.
5. Cost Savings: Detecting cancer early can save money on healthcare costs. Early-stage cancer is generally less complex to treat and requires fewer resources. This benefits both patients and healthcare systems.

In summary, the early diagnosis of cancer through the detection of key biomarkers is important because it provides more treatment choices, improves survival rates, allows personalized treatment decisions, reduces side effects, and saves money

on healthcare expenses. These potential benefits highlight the need for advancements in new tools to enable the early stage detection of these biomarkers.

As a result, this work aimed at developing a porous alumina-based electrochemical sensing platform for the sensitive detection of a target DNA, as a first step towards the detection of key miRNAs.

1.2 Sensing platform

Early detection of lung cancer is particularly challenging due to its often-latent nature during the initial stages. Consequently, there is a pressing need for sensitive and dependable tools for preclinical diagnosis. To address this need, numerous detection methods have been employed for early identification of lung cancer. As lung cancer tumors develop within the body, cancerous cells release specific biomarkers such as DNA, proteins, and metabolites. These biomarkers serve as indicators for the stages of lung cancer. Detecting and analyzing the levels of these biomarkers have proven valuable in screening and clinically diagnosing lung cancer [5] [6] [7].

Conventional methods for detecting lung cancer primarily involve imaging techniques such as X-rays, computed tomography (CT), and magnetic resonance imaging (MRI) [8]. While these methods are useful for identifying the presence and location of lung tumors, they have certain limitations. Firstly, they may not be effective in detecting small tumors in the early stages of the disease when the tumor size is below the detection threshold. Additionally, these imaging techniques do not provide information about the molecular characteristics of the tumor, such as specific biomarkers or genetic mutations, which can impact treatment decisions.

Advancements in new tools for the early stage detection of biomarkers, such as miRNAs, are crucial in improving cancer diagnosis and treatment outcomes. [9] [10][11].

The detection of free miRNAs in blood poses a challenge due to their low concentrations, necessitating highly sensitive detection tools. Therefore, the project aims to focus on the detection of exosomal miRNAs, which have emerged as powerful biomarkers for lung cancer. Exosomal miRNAs offer advantages as biomarkers, such as protection by the exosome lipid bilayer [12] and high concentrations in exosomal contents. However, exosomal miRNA detection is complicated: first, exosomes have to be isolated prior to detecting exosomal miRNAs.

Regarding exosomes isolation, ultracentrifugation has been conventionally used. While this techniques has some advantages, it also come with limitations and challenges [13]. Some of these limitations include:

1. High Cost: Ultracentrifugation machines are specialized equipment that can be expensive to purchase and maintain. The cost includes not only the equipment itself but also the necessary accessories and consumables.
2. Specialized Personnel: Operating ultracentrifugation machines requires technical expertise and specific knowledge. Skilled personnel are needed to configure and operate the equipment effectively, increasing the demand for specialized training.
3. Time-Consuming: Ultracentrifugation procedures at high speeds are time-consuming and laborious processes. The separation and concentration of biomarkers can take a significant amount of time, potentially delaying the analysis results.

4. Sample Volume Requirements: Ultracentrifugation techniques often require a considerable volume of the sample to achieve reliable results. This can be challenging when working with limited or precious samples, as the high centrifugal forces involved may damage or alter the samples.
5. Additional Tests for Interpretation: While ultracentrifugation can separate and concentrate specific biomarkers, further analysis may be necessary for accurate interpretation of the results. Techniques such as electrophoresis or mass spectrometry might be required to identify and characterize the separated biomarkers.

Once exosomes have been isolated, exosomal miRNAs have to be detected. PCR (Polymerase Chain Reaction) is a widely used technique for miRNA detection and offers several advantages for early-stage diagnosis as it allows for amplification of the target miRNA, increasing the signal and improving detection limits [14]. However, there are certain disadvantages of PCR. One major drawback is that PCR is a time-consuming technique, requiring several steps such as sample preparation, amplification, and analysis. The entire process can take hours to complete, which may delay the availability of results in urgent situations [15]. To overcome these limitations, biosensors have been shown as promising diagnostic tools, that can sensitively detect miRNAs, with a short analysis time and excellent accuracy.

Electrochemical biosensors present significant advantages over PCR for the early-stage diagnosis of lung cancer miRNA. Firstly, electrochemical biosensors offer rapid detection, providing real-time or near real-time results [16] [17]. This immediate availability of information enables prompt decision-making and timely intervention, which is crucial for early-stage diagnosis. Secondly, electrochemical biosensors exhibit portability and miniaturization potential, making them well-suited for point-of-care applications. Their compact size and ease of use allow for on-site testing and immediate results at the patient's location [16]. This mobility is particularly advantageous for early-stage lung cancer diagnosis, as it facilitates convenient and timely testing, leading to early detection and improved patient outcomes. Conversely, PCR typically requires specialized laboratory equipment and trained personnel, limiting its accessibility and applicability in decentralized healthcare settings [16].

To address the issues in detecting exosomal miRNA, the study aims to explore the potential of porous structures as a sensing platform for the electrochemical detection of exosomes and exosomal miRNAs associated with lung cancer. However, as an initial step, the focus is on developing the sensing component specifically for miRNA detection, which will be integrated with exosome capture and quantification in future work. This novel biosensor, enabling sequential detection of specific exosomes and target miRNAs, is expected to facilitate the accurate detection of small cell lung cancer in its early stages.

To fulfill the requirements of high sensitivity for detecting low miRNA concentrations and the ability to handle complex biological samples, porous alumina was chosen as the basis for the sensing platform in this project. The selection of porous alumina is justified by several factors. Firstly, the large surface area to volume ratio offered by the porous structure allows for a large active area, contributing to enhance the sensitivity. Secondly, employing a sensing mechanism based on measuring the pore blockage caused upon miRNA hybridization to the immobilized capture probe, has been demonstrated to improve sensitivity when compared to sensors based on flat electrodes. Lastly, the morphological features of the porous material can be leveraged to minimize interferences through size exclusion effects. In this project, porous alumina will be

fabricated, and its chemical functionalization will be tailored to serve as the sensing platform. Subsequently, the most suitable electrochemical detection mechanism for the target analyte, exosomal miRNAs, will be designed and optimized [11] [18].

In conclusion, the project focuses on the development of a porous material-based sensing platform with high sensitivity and compatibility to deal with complex biological samples. This platform aims to enable the electrochemical detection of target miRNAs, ultimately facilitating the accurate detection of small cell lung cancer in its early stages.

2 Materials and methods

The study aims to develop a sensor for DNA sensing, serving as an initial step towards designing a miRNA sensor, with pAAO (porous anodic aluminum oxide) being used as the substrate. The biosensor development process involves several sequential steps. Firstly, pAAO membranes are being fabricated to serve as the foundation for the sensor. Next, appropriate surface functionalization techniques are employed to enhance the sensor's performance. DNA conjugation is carried out to enable specific binding with the target molecules. Following that, carbon screen-printed electrodes are activated to ensure optimal electrochemical measurements. The electrochemical response is then measured using the developed biosensor. Lastly, detailed characterization of the substrate is being performed to assess its structural and functional properties. Each of these steps plays a crucial role in the development and performance of the DNA sensor, paving the way for future miRNA sensing applications.

2.1 Fabrication of porous alumina

The fabrication of porous alumina through electrochemical anodization is a widely used technique in various fields, including nanotechnology, electronics, and sensing applications. This process involves the controlled oxidation of aluminum in an electrolyte solution, resulting in the formation of a highly ordered array of nanopores within the alumina layer. The resulting porous alumina membranes possess unique properties such as high surface-to-volume ratio, tunable pore size, and excellent chemical stability [19].

2.1.1 Pre-treatment of aluminium substrate.

High-purity aluminum sheets, specifically high-purity aluminum foils with a purity of 99.999% obtained from Goodfellow Cambridge Ltd., were selected for the fabrication of porous alumina membranes. These aluminum foils had a thickness of 0.5 mm. To prepare the aluminum samples for anodization, they underwent a series of pre-treatment steps to ensure optimal surface conditions. Firstly, the aluminum sheets were carefully cut into squares measuring 2 cm x 2 cm, ensuring consistent sample sizes. Subsequently, the aluminum squares were subjected to a thorough cleaning process to remove any impurities. This process involved washing the samples with ethanol and water to eliminate any contaminants that may affect the anodization process. Furthermore, to achieve a pristine surface, the aluminum squares were degreased using acetone, ensuring the removal of any residual oils or greases. It is crucial to emphasize the flatness of the aluminum samples, as a flat surface is essential for obtaining a uniform and consistent porous alumina film during the subsequent anodization process.

Electrolyte	Anodization Control		Temperature	Voltage
	First Anodization	Second Anodization		
0.3 M Oxalic acid	Time control: 24 hours	Charge control: 2.27 C / µM / cm	5°C	40 V
0.3 M Sulfuric Acid	Time control: 24 hours	Charge control: 2.27 C / µM / cm	5°C	20 V
1 wt% Phosphoric acid	Time control: 24 hours	Charge control: 1.49 C / µM / cm	-6°C	195 V

Table 1. Anodization parameters for the fabrication of pAAO in different electrolytes.

2.1.2 Electropolishing

Electropolishing is a critical pre-treatment step performed on aluminum surfaces prior to the anodization process to achieve the desired quality and surface finish for the fabrication of porous anodic aluminum oxide (pAAO). This electrochemical process involves the controlled dissolution of the aluminum surface in an acidic electrolyte solution. By applying a specific voltage and current density, the aluminum surface undergoes anodic oxidation, resulting in the removal of surface imperfections, roughness, and contaminants. The electropolishing process enhances the surface smoothness, leveling out any irregularities or scratches that may exist on the aluminum substrate. This step plays a vital role in obtaining a mirror-like finish on the aluminum surface, ensuring uniform and consistent anodization during subsequent pAAO fabrication [20][21].

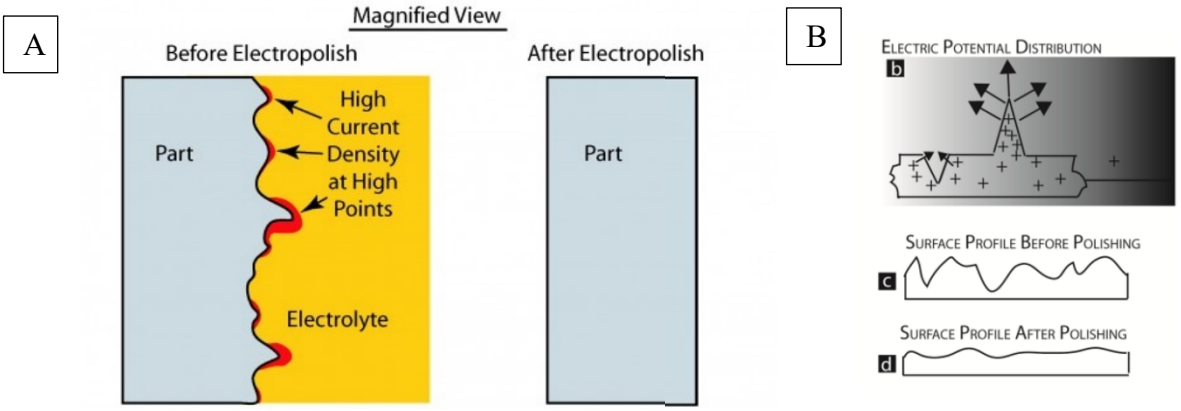

Figure 2. (A) Diagram of a substrate before and after being subjected to the electropolishing process adapted from [21] and (B) scheme of the electropolishing process adapted from [20].

This process is carried out in an electrochemical cell whose components are:

- Anode
- Cathode
- External DC circuit
- Electrolytic solution

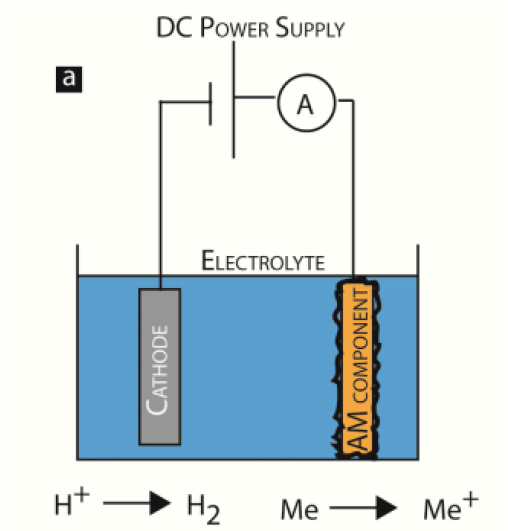

Figure 3. Components of an electrochemical cell adapted from [22].

The electrical current scheme is as follows.

- The four aluminum sections will be connected to the positive terminal of the power supply, therefore they will be positively charged thus acting as anode. The anode, being a metal, undergoes an oxidation reaction. When being oxidized, the aluminum ionizes and enters the electrolytic solution causing corrosion of the anode, while simultaneously the electrons leave the anode through the electrolytic solution [23].

- The negative charge is found in a platinum filament, acting as the cathode, which is connected to the negative terminal of the power supply. The reduction reaction takes place at the cathode. Here the metal ions formed in the oxidation reaction combine with electrons at the cathode by coating the platinum surface, or by dissolving in the electrolytic medium [23].

The electrolytic solution is a conductive liquid which acts as a medium for the metal ions so that these ions leave the cathode surface and go to the anode to be deposited there.

The system that has been used is as seen in Figure 4.

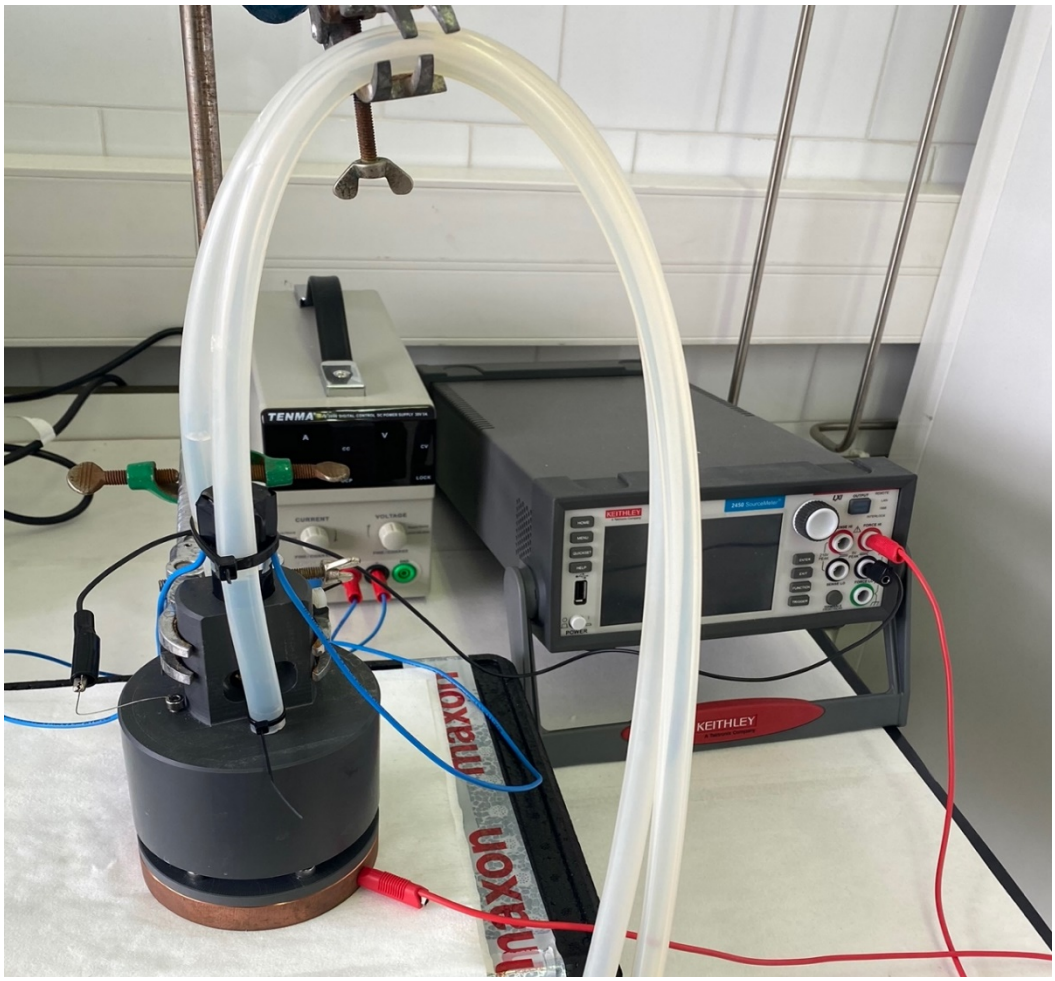

Figure 4. Electrochemical fabrication setup.

During the electropolishing process, the aluminum substrate undergoes a controlled electrochemical reaction to obtain a mirror-like surface [21]. In this particular method, the aluminum was electropolished for 6 minutes at 20 V in a solution of $HClO_4$ and ethanol (1:8, v/v), with the stirring direction alternated every minute. The process was carefully carried out at a temperature of 4°C, which was essential for maintaining optimal reaction conditions. The low temperature helps controlling the electrochemical reaction kinetics, preventing excessive heat generation and minimizing the risk of thermal damage or distortion to the aluminum surface. Additionally, the controlled temperature ensures a stable electrolyte solution, facilitating precise control over the electropolishing process and resulting in the desired surface smoothness.

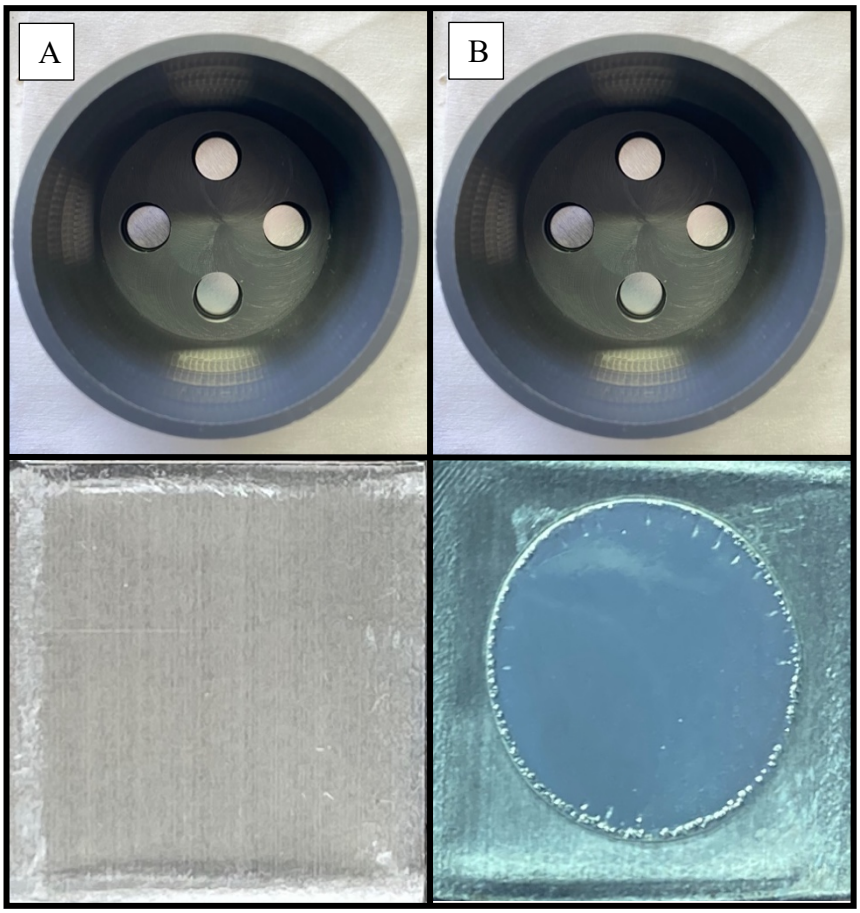

Figure 5. Samples prior to the process (A) and samples after the electropolishing process (B).

2.1.3 First anodization

The first anodization is a crucial step in the fabrication of pAAO membranes. It involves exposing the aluminum substrate to an electrolyte solution and applying a controlled voltage to induce an oxidation reaction at the surface. The choice of electrolyte depends on the desired properties and characteristics of the pAAO. During the first anodization, a thin and ordered oxide layer called the barrier layer is formed on the aluminum surface. This barrier layer acts as a protective coating, preventing further oxidation of the aluminum substrate. The thickness of the barrier layer can be controlled by adjusting the anodization parameters, including voltage, temperature, and anodization time.

The first anodization plays a crucial role in determining the pore size and distribution in the resulting pAAO. By carefully selecting the anodization conditions, desired pore size range, typically ranging from nanometers to micrometers, can be achieved. The pore size and distribution are influenced by factors such as the electrolyte composition, temperature, and applied voltage.

The first anodization process requires precise control and monitoring to ensure uniform and reproducible results. Maintaining a stable anodization temperature is

particularly important as it can affect the growth rate and morphology of the barrier layer.

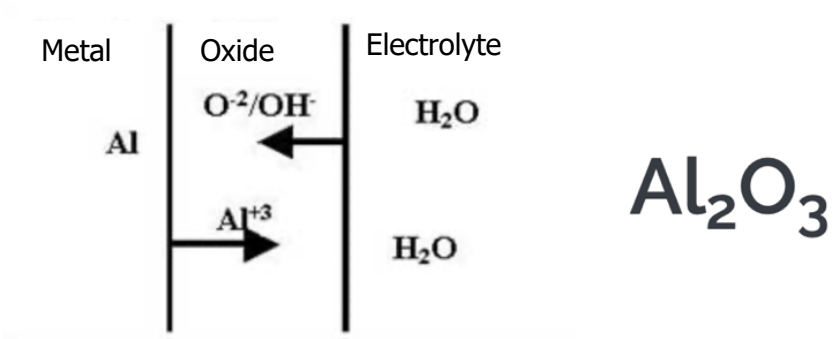

Figure 6. Reaction for alumina formation adapted from [24].

Three different electrolytes are used to fabricate pAAO depending on the pore size required for the sensing platform:

- Sulphuric acid to obtain pore sizes between 15 to 40 nm.
- Oxalic acid to obtain pore sizes between 30 to 80 nm
- Phosphoric acid to obtain pore sizes between 90 to 400 nm.

pAAO membranes are fabricated using different electrolytes to meet specific sensing requirements. For instance, anodization in oxalic acid electrolyte at 40 V and 5°C is commonly employed. Under these controlled conditions, aluminum substrates undergo anodization, resulting in the formation of highly ordered and regular pore arrays within the alumina layer. The pore size and density can be precisely controlled. Similarly, anodization in sulfuric acid electrolyte at 20 V and 5°C is utilized for the production of pAAO membranes with smaller pore sizes. Additionally, anodizing aluminum in phosphoric acid electrolyte is done under mild anodization – hard anodization conditions, where the aluminium is subjected to a potential of 175 V to form an oxide passivation which helps avoid the breakdown of the pAAO layer formed under hard anodization condition at 195 V and -6°C.

A typical current – time transient of first anodization aluminium under potentiostatic conditions can be seen in Graph 1. When the potential is applied to the system, in the primary phase the sudden drop in current represents a formation of a thin barrier oxide layer. Due to the barrier layer there are instabilities in the electric field across the film and the oxide film starts to partially dissolve on specific sites, known as nucleation centers. The pore formation starts at these nucleation centers on the aluminium-aluminium oxide interface. Finally the current density settles to a constant value, where the pore growth is under steady state.

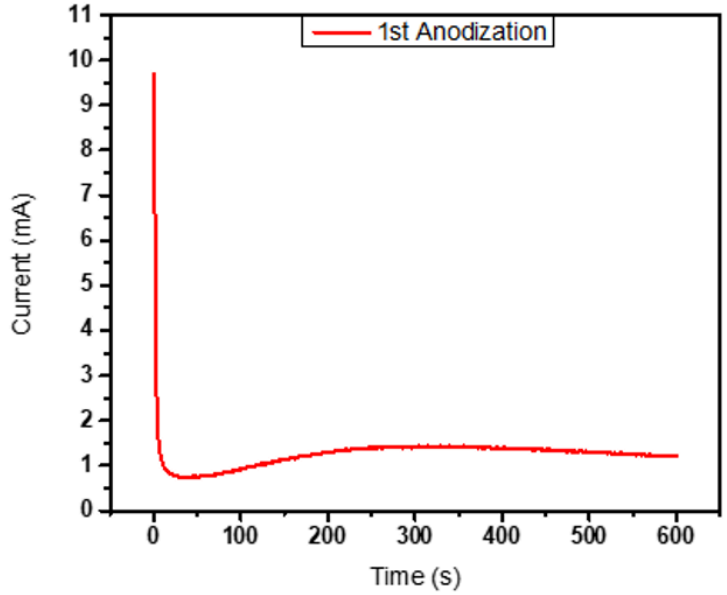

Graph 1. Current-time transient at constant potential during first anodization.

2.1.4 Etching of unordered pores

The etching process serves to remove the unordered porous alumina (pAAO) film, leaving behind an aluminum template with highly organized concavities. These concavities act as the starting points for the pore initiation during the second anodization step, playing a crucial role in the formation of an ordered pAAO film.

Following the first anodization, the cell and the four samples underwent a thorough cleaning procedure. They were carefully washed with deionized water, followed by ethanol, and dried using compressed air. Subsequently, the four samples were placed in a beaker.

To initiate the etching process, a heated acidic solution containing chromic acid and phosphoric acid in a ratio of 6 wt% to 1.8 wt% was prepared. The solution was poured into the beaker, which was then placed on a magnetic stirrer equipped with a heating plate. The temperature of the solution was set to 70°C, as monitored by a thermometer immersed in the solution. The magnetic stirrer provided continuous agitation to the acid solution, ensuring uniform heating and mixing. This agitation process was maintained for one hour, allowing the solution to effectively remove the disordered porous alumina layer. As a result, concavities were formed, serving as molds for the growth of new, ordered pores.

Figure 7. Etching system.

2.1.5 Second anodization

Following the first anodization, the aluminum surface displays irregular hexagonal pores. To achieve ordered concavities with improved pore regularity and without imperfections, a chemical etching step is performed to remove the unordered porous alumina. This process effectively eliminates the irregular pores, leaving behind concavities on the aluminum substrate that serve as growth sites for the pores during the second anodization. Consequently, the subsequent anodization process results in enhanced pore regularity.

Similar to the first anodization, the aluminum substrates were clamped between the PVC cell and the copper plate. It is important to note that both the first and second anodizations were conducted at the same anodization voltage.

For the fabrication of porous alumina membranes using oxalic acid and sulfuric acid, a charge of 2.27 C per cm^2 was necessary to grow a film with a thickness of 1 µm. On the other hand, the fabrication of pAAO with phosphoric acid required a charge of 1.49 C per cm^2 to achieve the same 1 µm thickness. These varying charge requirements highlight the influence of the electrolyte on the growth kinetics and resulting thickness of the pAAO membranes.

By carefully controlling the charge accumulation during the second anodization, precise control over the thickness of the resulting porous alumina membranes was achieved. This control is crucial in tailoring the membranes to meet specific sensing requirements, ensuring consistent and reproducible results. Graph 2 displays a typical second anodization (a) current – time, (b) thickness – time, and (c) total charge – time profile during the second anodization of aluminium with oxalic acid.

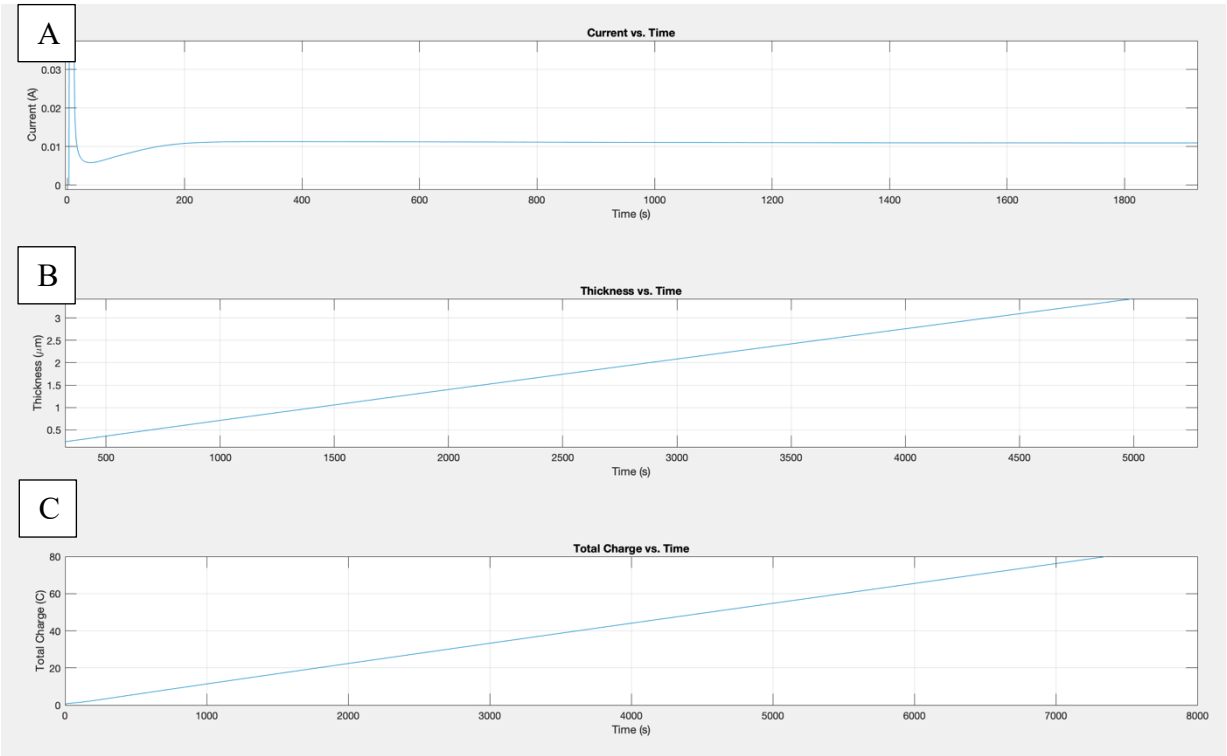

Graph 2. Typical second anodization (a) current – time, (b) thickness – time and (c) total charge – time profile during the second anodization of aluminium with oxalic acid.

2.1.6 Chemical etching of aluminum

The removal of aluminum from the pAAO film is a critical step that allows for the subsequent wet chemical etching of the barrier oxide layer. This process is important because it exposes the barrier oxide layer, which is necessary for further manipulation and modification of the pAAO structure.

To remove the aluminum, a selective dissolution process is employed. One common method is to use a saturated acid solution of a suitable etchant, such as copper chloride ($CuCl_2$) and hydrochloric acid (HCl). The aluminum is dissolved in the etchant solution, while the barrier oxide layer remains intact. By removing the aluminum, the barrier oxide layer becomes exposed and accessible for further characterization or modification. This is essential for studying the chemical composition, analyzing impurities, or conducting additional processes on the barrier layer.

Once the above processes have been completed, four samples were obtained which had a layer formed by alumina which contained ordered pores as shown in Figure 8.

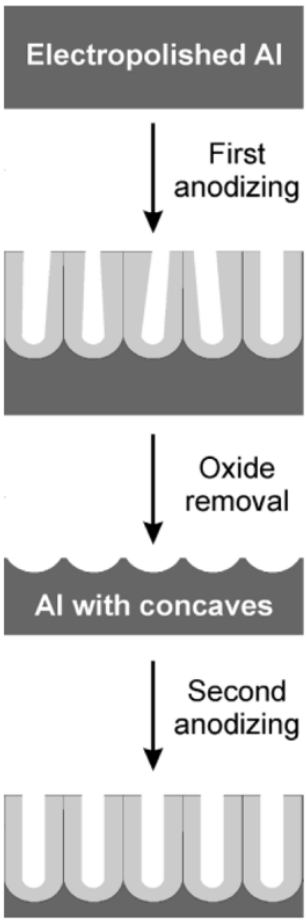

Figure 8. Scheme of the pAAO formation by electrochemical anodization of aluminium adapted from [25] .

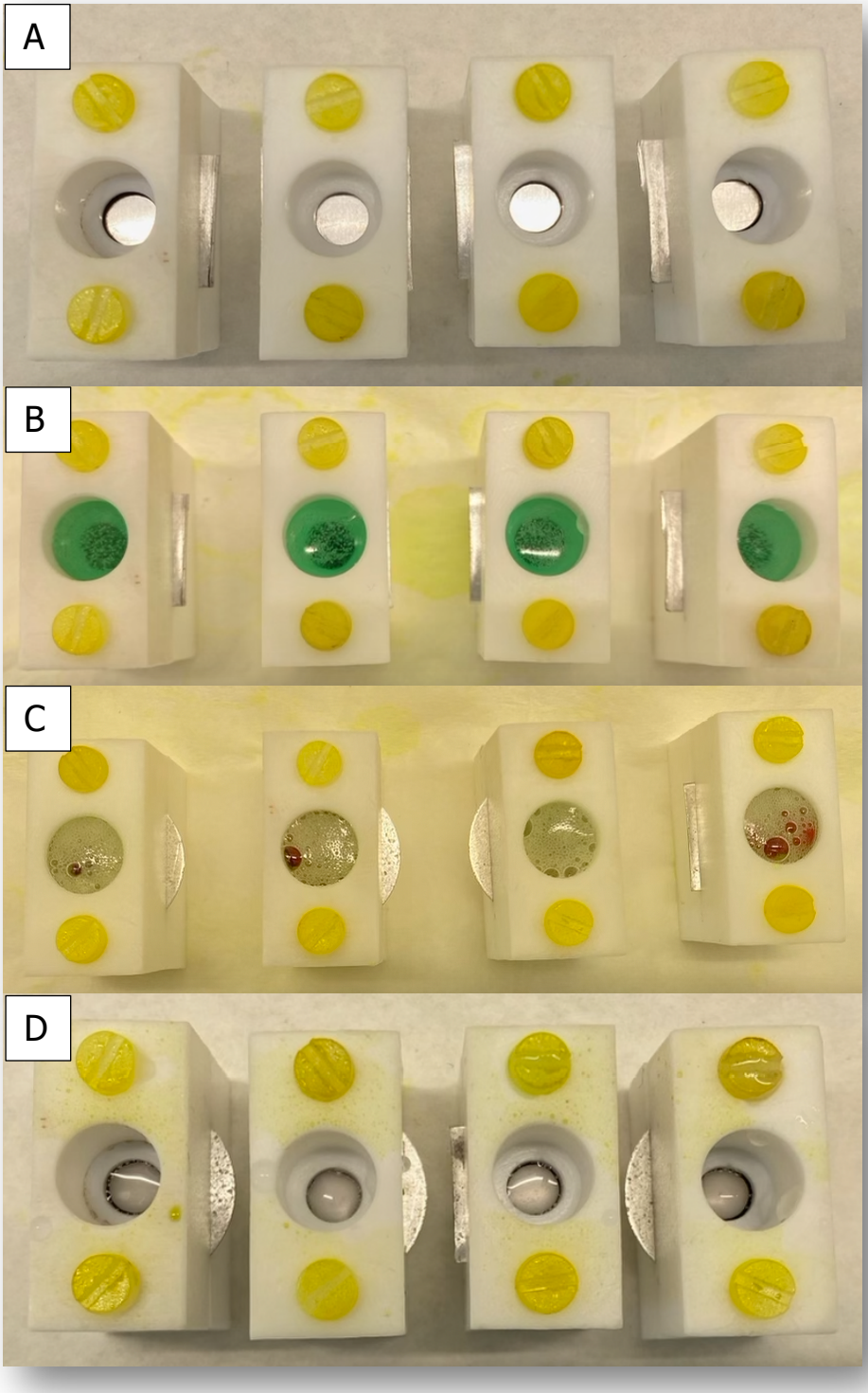

Figure 9. (A) Clamping aluminium samples upside-down, (B) immediately after adding $CuCl_2$ and HCl, (C) after 10 minutes and (D) complete removal of aluminium.

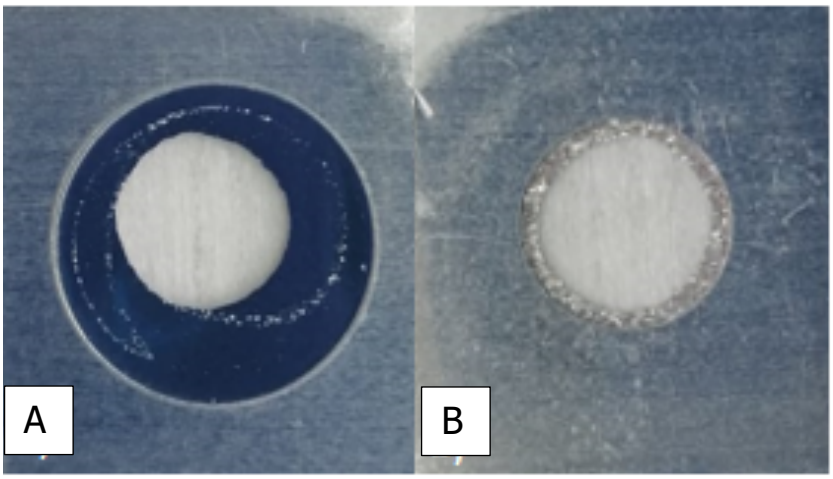

Figure 10. Aluminium samples after etchinf of aluminium. (A) Front side of the aluminium and (B) back side of the alumium etched. As can be seen, the difference between the two images is that in (A) there is aluminium, while in (B) the aluminium has been removed.

This resulted in four samples composed of a nanoporous alumina layer and the barrier layer.

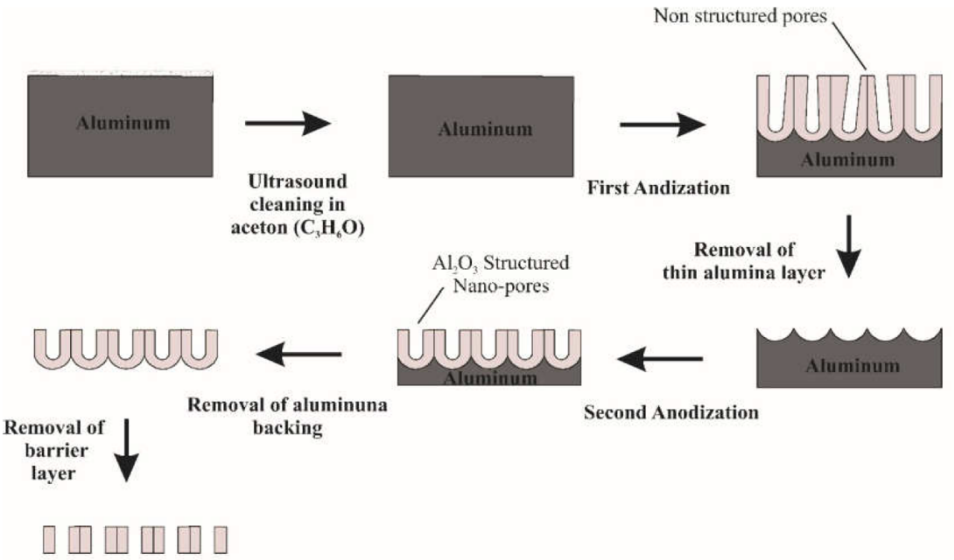

Figure 11. Scheme of the two-step anodization process for the fabrication of a pAAO membrane adapted from [26].

2.1.7 Barrier oxide layer removal

Once the aluminium layer has been removed, it is necessary to remove the barrier layer to obtain the pAAO membrane.

The wet chemical etching of the barrier oxide layer plays a crucial role in the fabrication of pAAO membranes. After the aluminum removal step, the barrier oxide layer is exposed and ready for etching. This process involves immersing the sample in a suitable etchant solution that selectively dissolves the barrier oxide layer while leaving the porous structure intact. During the etching process, the etchant solution chemically reacts with the barrier oxide layer, gradually removing it from the surface of the pAAO film. The etchant selectively attacks the barrier oxide layer due to its different chemical composition compared to the porous structure. This selective removal allows for precise

control over the pore dimensions, pore density, and surface properties of the resulting pAAO membrane.

By adjusting the etching time and the concentration of the etchant solution, the pore dimensions and pore density can be modified. Etching for a longer duration leads to larger pores and reduced pore density, while shorter etching times result in smaller pores and higher pore density. This ability to control the pore dimensions and pore density is highly advantageous, as it allows for tailoring the membrane's characteristics to meet specific application requirements [27].

2.2 Functionalization

The functionalization of pAAO membranes is a critical aspect of their utilization for biosensing applications [11]. To enable the selective and sensitive detection of target analytes, the membranes must be functionalized to allow the covalent binding of specific bioreceptors [28][11]. These bioreceptors, such as antibodies, enzymes, or DNA strands, serve as recognition elements that interact with the target molecules of interest. The functionalization process involves introducing suitable functional groups onto the membrane surface to allow the immobilization of the carefully selected bioreceptors.

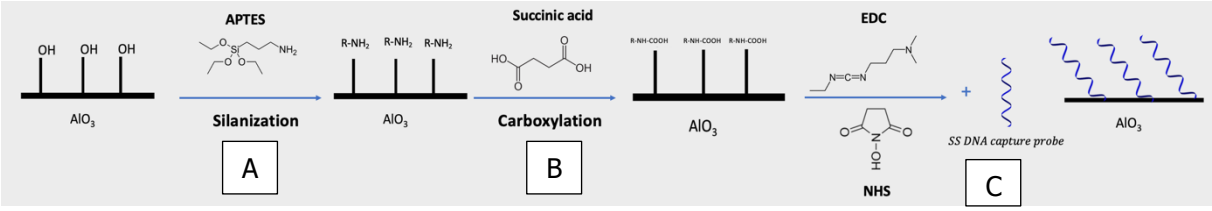

Figure 12. Functionalization scheme. (A) Silanization with APTES. (B) Succinic acid binding for carboxylation, and (C) EDC/NHS activation and ssDNA conjugation.

2.2.1 Hydroxylation

Hydroxylation of pAAO membranes is a key step to allow their subsequent functionalization via silanization. To introduce hydroxyl (OH) groups on the surface of pAAO, a hydroxylation process was carried out. Initially, the pAAO substrates underwent a thorough cleaning procedure using water and ethanol. An oil bath was preheated to 180 ºC, while the temperature of the hydrogen peroxide (H_2O_2) solution was maintained at 100 ºC. The substrates were then immersed in a 30% aqueous H_2O_2 solution at 160 ºC (corresponding to the temperature of the oil bath) for a duration of 1 hour. Subsequently, the pAAO samples were carefully removed from the solution and transferred directly to an oven set at 60 ºC. The samples were allowed to dry in the oven for a period of 2 hours, facilitating the completion of the hydroxylation process.

2.2.2 Silanization

After the introduction of -OH group on the surface, the pAAO substrates were carefully transferred to a teflon holder placed inside a Schlenk flask, which was then sealed with a rubber stopper to maintain a controlled environment. To initiate the silanization process, 99.85% extra-dry toluene was injected into the flask using a syringe while ensuring a constant flow of nitrogen. The reaction temperature was carefully maintained at 28 ºC throughout the procedure. The wet-chemical silanization route was employed in a moisture-free environment, utilizing a solution of (3-aminopropyl) triethoxysilane (APTES) in dry toluene (5% v/v) for a duration of 30 minutes. Following the silanization step, the substrate was removed and rinsed with toluene to remove any excess reagents, then dried using a stream of nitrogen gas. Subsequently, the

membranes were placed in an oven and dried for 1 hour at 100 ºC. Finally, the dried membranes were carefully stored under vacuum conditions until further use.

2.2.3 Carboxylation

After the successful introduction of amine groups through the functionalization of the membranes with APTES, the subsequent step involved carboxylation to create amide (CO-NH_2) bonds and leave a free COOH group for further functionalization.

To achieve carboxylation, a 0.2 M solution of succinic acid in dimethyl sulfoxide (DMSO) was prepared. Succinic acid, a dicarboxylic acid, contains two carboxylic acid functional groups (-COOH). The amine groups present on the membrane surface from the APTES functionalization reacted with the succinic acid molecules, resulting in the formation of amide bonds. This chemical reaction is known as amide bond formation, where the amine group (-NH_2) of APTES reacts with the carboxylic acid group (-COOH) of succinic acid.

During the carboxylation process, the COOH groups of succinic acid were effectively tethered to the amine-functionalized membrane surface, introducing new functional groups. These COOH groups provide reactive sites for further functionalization, including the covalent binding of antibodies, facilitating the specific detection and sensing of target molecules in biosensing applications.

2.2.4 DNA conjugation

To covalently bind an amine-modified DNA capture probe to the COOH-modified pAAO surface, carbodiimide chemistry was used. Two solutions were prepared for this reaction: a 10 mg/mL N-(3-dimethylaminopropyl)-N'-ethylcarbodiimide hydrochloride (EDC) solution, and a 15 mg/mL N-hydroxysuccinimide (NHS) solution, both prepared in 0.1 M MES buffer, adjusted to a pH of 5.4. Next, these solutions were combined in a 1:1 (v/v) ratio.

The pAAO substrates, previously subjected to the carboxylation process, were arranged in a petri dish. The EDC-NHS solution was carefully poured over each substrate, ensuring complete coverage. To promote efficient reaction kinetics, the petri dish was placed on a shaker and allowed to react for a period of 30 minutes.

EDC and NHS molecules in the solution react with the carboxyl groups on the pAAO membrane surface, forming active ester intermediates. These intermediates provide reactive sites for subsequent conjugation reactions, facilitating the attachment of biomolecules, such as single-stranded DNA (ssDNA). The EDC-NHS chemistry employed in this study is well-known for its effectiveness in activating carboxyl groups for conjugation purposes. By utilizing this chemistry, the functionalization of the pAAO membranes with specific biomolecules becomes feasible. In the context of ssDNA conjugation, the activated carboxyl groups serve as anchor points for the covalent attachment of amine-modified ssDNA molecules, allowing for the introduction of specific ssDNA capture probes onto the membrane surface [11] [28]. The EDC-NHS activated pAAO membranes were incubated with a 100 µM solution of 0.5 µM solution of amine-modified ssDNA capture probe (5´-NH_2-C6-TGGGGTCAAACTGACA-3´) prepared in 0.1 M phosphate-buffered saline (PBS) and the same volume of 0.5 µM solution of a random amine-modified ssDNA sequence (5'-NH_2-C6-AGTTATCCCAGTCTTATAGGTAGGT-3') prepared in 0.1 M PBS for controls for a period of 1 hour at room temperature on a shaker followed by overnight incubation at 4 ºC.

2.2.5 Surface blocking

To ensure surface blocking and minimize non-specific binding, each sensor was subjected to incubation in ethanolamine. A volume of 300 µL of 0.1 M ethanolamine, prepared in 0.1 M PBS at a pH of 7.4, was dispensed onto each sensor. This incubation was carried out for a duration of 1 hour at room temperature, utilizing a shaker for consistent agitation. The use of ethanolamine as a blocking agent helps to block any remaining unreacted sites on the sensor surface, reducing the likelihood of non-specific interactions and enhancing the specificity of subsequent analyte binding [29].

2.3 Electrochemical techniques

Electrochemical measurements were performed using a custom-built 3-electrode electrochemical teflon cell. The electrochemical cell comprised of a pAAO substrate as sensor platform on a carbon screen-printed electrode acting as working electrode, a Pt counter electrode, and a Ag/AgCl reference electrode.

Initially, stability measurements were done to ensure a stable baseline signal from the sensor and control electrodes. For stability measurements, up to 5 cycles of cyclic voltammetry, electrochemical impedance spectroscopy and square wave voltammetry were recorded with incubation of approximately 30 minutes between each measurement. The electrochemical measurements were performed in an electrolyte solution (730 µL) of 2 mM $K_4[Fe(CN)_6]$ and 2 mM $K_3[Fe(CN)_6]$ prepared in 0.1 M PBS. The sensors were considered stable when at least 2 consecutive measurements were similar to each other.

After the sensing platform was stable, the sensor cells and control cells were washed thoroughly and incubated with different concentrations (0.1 pM, 1 pM, 10 pM, 100 pM and 1000 pM) of the target ssDNA (5'- TGTCAGTTTGACCCCA -3') for 30 minutes each. After incubation with each concentration, cyclic voltammetry, electrochemical impedance spectroscopy and square wave voltammetry measurements were performed.

2.3.1 Cyclic Voltammetry

Cyclic Voltammetry (CV) is a widely used electrochemical technique that allows the investigation of reduction and oxidation processes of electroactive species. In CV, the potential of the working electrode is linearly ramped with respect to time. Once the set potential is reached, the potential of the working electrode is ramped in the opposite direction to return to the initial potential. This cyclic process can be repeated multiple times (as shown in Figure 13). The resulting current at the working electrode is plotted against the applied voltage, producing a cyclic voltammogram trace that provides valuable insights into the electrochemical properties of the analyte.

In a cyclic voltammogram, the x-axis represents the imposed parameter on the system, which is the applied potential (E), while the y-axis represents the resulting current (I). The two peaks observed in the voltammogram correspond to the peak oxidation current (Iox) and peak reduction current (Ired) at the oxidation potential (Eox) and reduction potential (Ered), respectively. The difference between these two peaks is referred to as the peak-to-peak potential separation (ΔEp).

For the CV measurements in this study, the following conditions were employed: an initial potential (Estart) of -0.5 V, a potential range from 0.8 V to -0.5 V, a potential step (Estep) of 5 mV, three cycles of potential sweeping, a current range of 1 mA, and a scan rate of 100 mV/s. These parameters were carefully selected to ensure accurate and reliable characterization of the electrochemical behavior of the analyte.

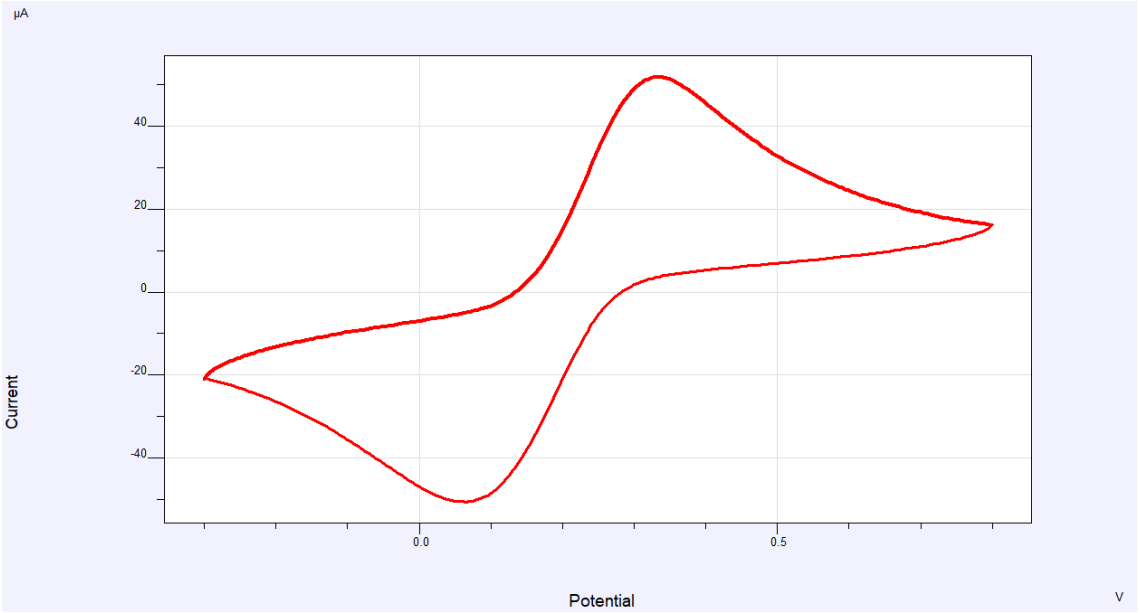

Figure 13. Example of a CV graph.

2.3.2 Square wave voltammetry

Square Wave Voltammetry (SWV) is a highly sensitive electrochemical technique that offers excellent signal-to-noise ratio by isolating the faradaic signal contribution and minimizing the effects of eddy currents. It utilizes a symmetrical square wave pulse superimposed on a staircase wave, resulting in a distinctive square wave pattern (Figure 14). The pulse duration (τ) corresponds to the staircase length, and the forward pulse of the square wave aligns with the first half of the staircase. Key parameters in SWV include Esw, the height of the square wave pulse, and Esc, the staircase rise for each step.

The measured current signal in SWV is derived from the difference between two experimentally obtained currents. The first current is recorded at the end of the forward square wave pulse, while the second current is measured at the end of the return square wave pulse. This subtraction of currents with opposite signs enhances the peak height, resulting in sharper and more defined peaks in the voltammogram.

For the SWV measurements in this study, the following conditions were utilized: an initial potential (Estart) of -0.2 V, a final potential (Eends) of 0.8 V, a potential step (Estep) of 5 mV, one cycle of the square wave pulse, a current range of 100 µA, a square wave frequency of 5 Hz, and a pulse amplitude of 25 mV. These carefully chosen parameters allowed for accurate and reliable analysis of the electrochemical behavior, facilitating the identification of characteristic peaks and trends in the SWV voltammogram.

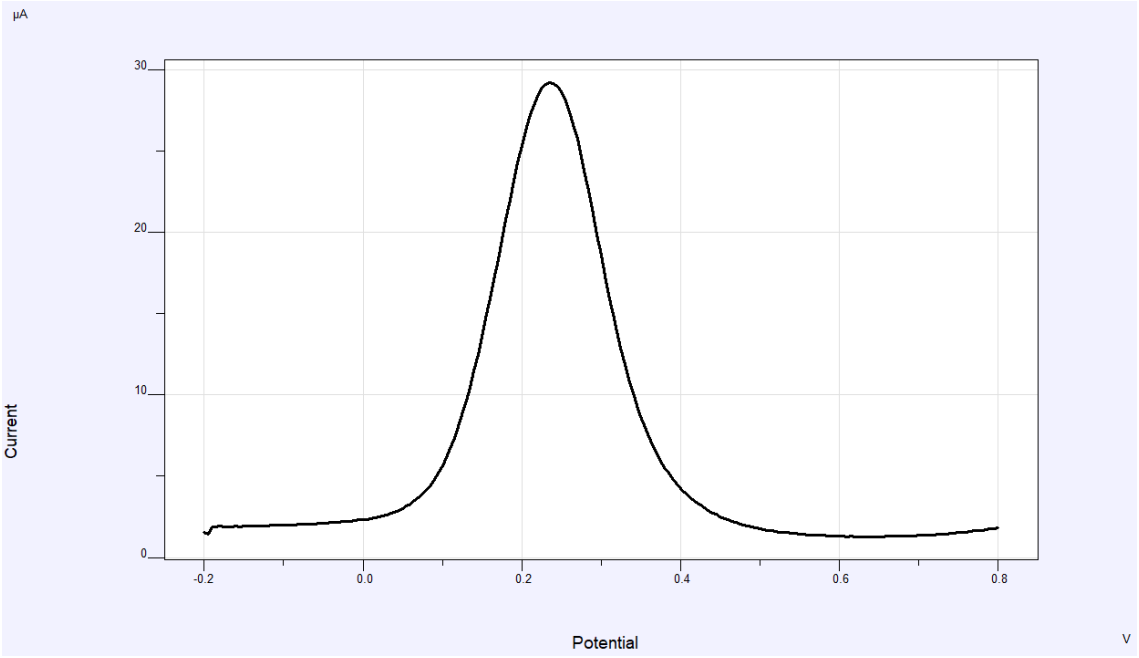

Figure 14. Example of a square wave voltammogram.

2.3.3 Electrochemical impedance spectroscopy

Electrochemical Impedance Spectroscopy (EIS) is a versatile technique for investigating capacitive, inductive, and diffusion processes within an electrochemical cell (Figure 15). By applying a low-amplitude alternating current (AC) signal, EIS enables the analysis of cell impedance characteristics. Unlike single-frequency measurements, EIS involves acquiring impedance data at multiple frequencies, resulting in an impedance spectrum. This spectrum provides valuable insights into surface phenomena, changes in bulk properties, as well as exchange and diffusion processes.

For EIS measurements, the following conditions were employed: Estart = 0.2 V, 51 frequencies, and a current range of 100 µA. These settings allowed for comprehensive characterization of the electrochemical system, facilitating the evaluation of various processes and phenomena across a broad frequency range.

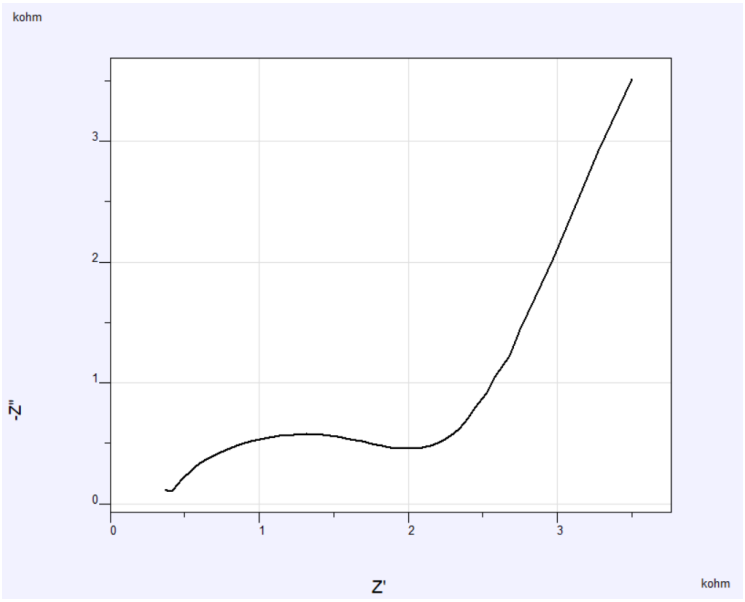

Figure 15. Example of an EIS spectrum.

2.3.4 Activation of carbon screen-printed electrodes (C-SPE)

C-SPE electrodes from Quasense required activation before their utilization to achieve a consistent electrochemical response. Activation was conducted by subjecting the C-SPE to amperometry in a 0.05 M carbonate buffer solution at pH 9.6, applying a potential of 1.2 V for 45 seconds. Following each amperometry cycle, CV was performed in a 2 mM ferrocyanide and 2 mM ferricyanide solution prepared in PBS at pH 7.4. The third cyclic voltammogram for each step was recorded both before activation and after each activation cycle. Activation cycles were repeated until cyclic voltammograms from two consecutive activation steps exhibited similarity, indicating successful electrode activation.

2.4 Characterization of porous alumina membranes

2.4.1 SEM

The Scanning Electron Microscope (SEM) is a highly versatile instrument that offers valuable insights into surface topography and chemical composition. In this study, SEM was employed as a characterization technique to assess the pore size and thickness of the membranes. By examining these parameters, it was possible to determine whether the fabrication processes yielded the desired outcomes.

2.4.2 FTIR

Infrared spectroscopy is a vibrational spectroscopic technique that provides valuable information about the functional groups present in a sample. The IR spectrum plots the absorbance or transmittance of infrared radiation on the y-axis against the scanning wavelength on the x-axis. Molecules in the sample exhibit absorption at specific frequencies that are characteristic of their oscillating frequencies, reflecting the unique structure of the molecule. This absorption frequency corresponds to the transition energy of the vibrating bond or functional group.

For the FTIR characterization of our porous membranes at each step of the modification process, an FTIR spectrometer/Jasco 600 system (Figure 16) was utilized. This system is equipped to collect spectral data in the mid-infrared (MIR) region. Throughout the functionalization process, the FTIR technique was employed to verify the successful covalent binding of the ssDNA capture probe to the membrane surface. Since the technique is qualitative in nature, it facilitated the analysis of the functional groups introduced onto the membrane surface at each step.

Reflectance spectroscopy, along with a liquid nitrogen-cooled MCT detector, was employed to capture the spectra. All spectra were obtained as an average of 64 scans, with a resolution of 4 cm^{-1}, covering the range of 450-4000 cm^{-1}. To correct the raw spectra, background in air was utilized.

Figure 16. Jasco FT/IR-6700, used for recording IR spectra.

3 Results and discussion

PAAO-based sensing platforms have some advantages over other nanoporous material-based sensing platforms (such as porous silicon and porous silica). As pAAO is made through self-ordering electrochemical anodization, it produces uniform and parallel nanochannels. pAAO structures' uniformity and homogeneity contribute to their reproducibility, resulting in sensing platforms that can provide accurate and reliable sensing results. pAAO also has high chemical, thermal, and mechanical stability, as well as excellent biocompatibility, which overcomes some of the limitations of other types of porous materials.

Since it has high sensitivity and short detection time, electrochemical detection is a powerful transduction method. Most importantly, electrochemical transduction allows for smart point-of-care device miniaturization.

To that end, we combine the advantages of electrochemical sensing with the adaptability of pAAO to create a sensing platform for miRNA detection. When compared to flat electrodes, the pAAO membrane-modified electrode functionalized with ssDNA capture probes within the nanochannels effectively increases the number of available biorecognition elements and thus offers improved sensing performance.

The partial or complete blockage of pAAO nanochannels as a result of analyte specific binding to capture probes immobilized within the pores (as seen in Figure 17) has been used as a sensing strategy for direct and label-free electrochemical detection

of various biomolecules. A blocking event obstructs the diffusion of an electroactive species added in solution to the electrode surface, resulting in a decrease in oxidation current. Using a pAAO membrane to modify electrodes makes it easier to implement this versatile sensing strategy.

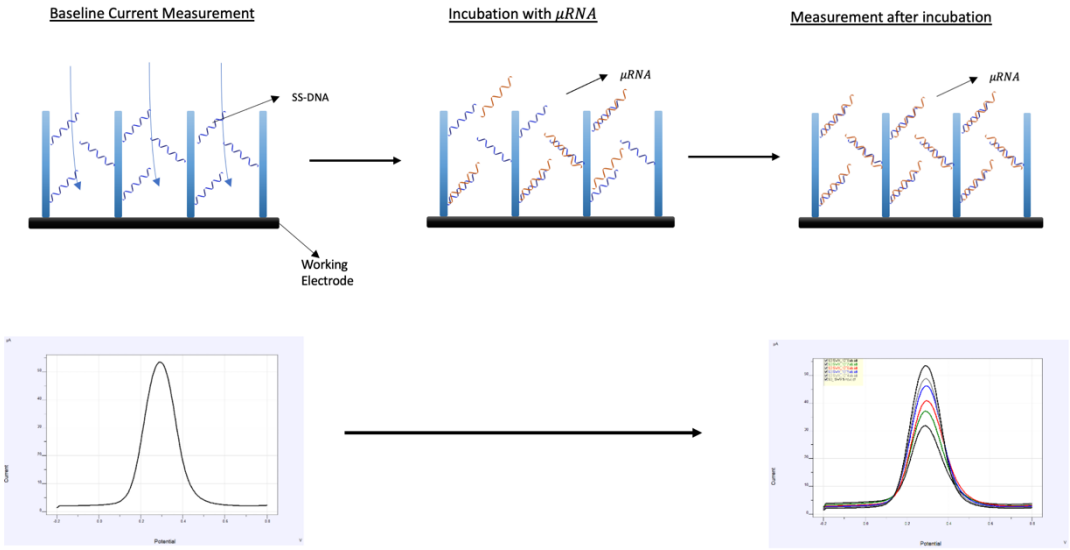

Figure 17. Schematic of the sensing mechanism based on pore blockage.

3.1 Characterization results

pAAO membranes fabricated with oxalic acid were employed for sensing experiments, and thus the morphological characterization, was performed, via SEM to verify the pore size diameter. Control over the pore size of the nanochannels is vital as it provides for effective blockage of nanochannels with binding of the target analyte to the bioreceptor immobilized in the pAAO. These membranes were later functionalized, followed by covalent immobilization of the ssDNA capture probe prior to sensing via electrochemical measurements. At each step of surface modification, these membranes were characterized using IR spectroscopy.

3.1.1 SEM analysis

The DNA sensing experiments were performed using fabricated membranes with pore size of 40 nm ± 5 nm and 50 nm ± 5 nm for front and back side, respectively (Figure 18). Previous optimizations on the platform revealed this specific pore size to achieve the highest sensitivity. The fabrication conditions are the ones discussed in Material and methods sections of this thesis.

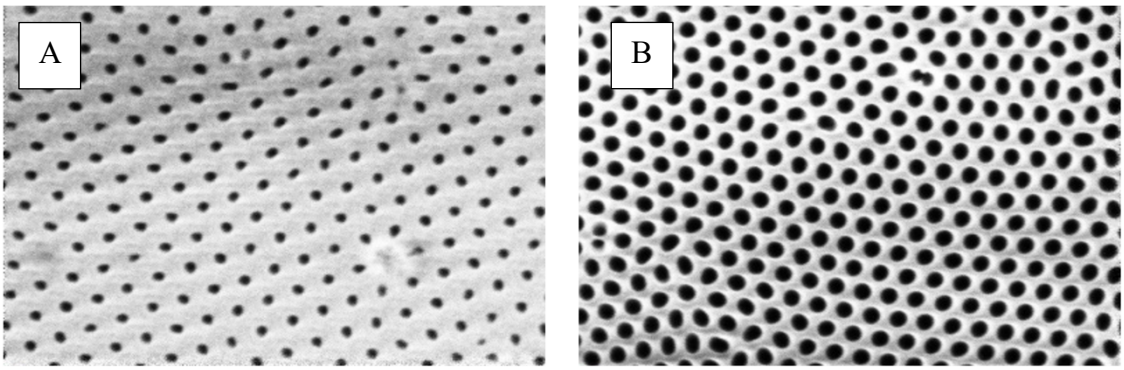

Figure 18. (A) Before pore widening (after barrier layer removal), and (B) after pore widening (20 minutes).

3.1.2 IR Spectra

Infrared spectroscopy was used as a qualitative technique to identify the functional groups stepwise introduced on the pAAO substrate.

IR was recorded at each step of membrane modification to confirm the presence of the expected functional groups. These include:

- **Hydroxylation**

  To allow silanization, the presence of OH groups on the surface of pAAO is necessary. Therefore, hydroxylation is performed using hydrogen peroxide to introduce these functional groups initially. Figure 19 shows the reflectance spectrum associated with this step, in which a broad band around 3400 cm^{-1} is observed, which is attributed to the stretching of the OH bonds.

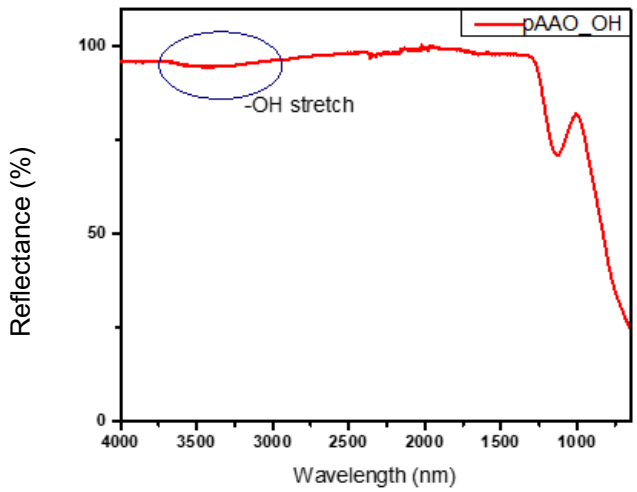

Figure 19. Reflectance spectrum of hydroxylated pAAO substrate shows the OH stretch at ~3400 cm^{-1}.

- **Silanization**

  Silanization was done with 5% (v/v) ratio of APTES in extra dry toluene under N_2 atmosphere for 30 minutes. A characteristic double peak at 2854 cm^{-1} and 2916 cm^{-1} was observed as shown in Figure 20, which corresponds to the presence of C-H stretching from the methoxy groups.

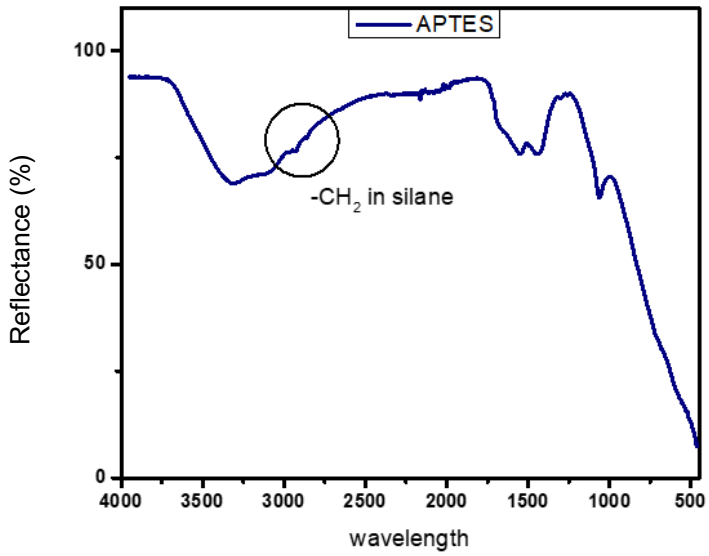

Figure 20. Reflectance spectrum of an APTES-silanized pAAO substrate.

- **Succinic acid treatment**

  Incubations of the silanized membranes with a solution consisting of 0.2 M succinic acid in DMSO and 0.1 M sodium bicarbonate at pH 9.4 were carried out in order to introduce carboxyl groups into the pAAO samples. During this process, new peaks were observed at 1631 cm^{-1}, corresponding to the amide bond, and at 1457 cm^{-1}, corresponding to the carbonyl group. This can be seen in Figure 21.

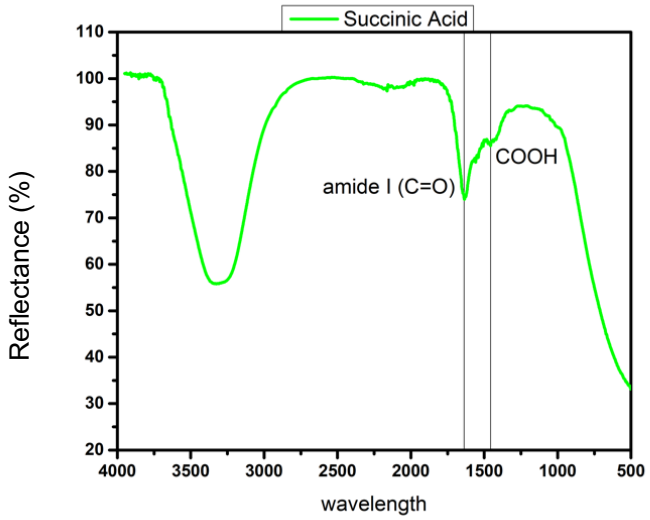

Figure 21. Reflectance spectrum of an APTES-silanized pAAO substrate upon reaction with succinic acid.

- **EDC/NHS activation and immobilization of ssDNA capture probe**

  EDC (1-ethyl-3-(3-dimethylaminopropyl) carbodiimide) was used to react with the carboxylic acid groups on the pAAO surface, which generated o-acylisourea. This o-acylisourea then reacted with NHS (N-hydroxysuccinimide) to form an NHS ester, which subsequently bound to the amine-terminated ssDNA probe. Figure 22 shows a comparison of the FTIR spectra recorded after DNA

conjugation in relation to the spectra obtained in each previous functionalisation step.

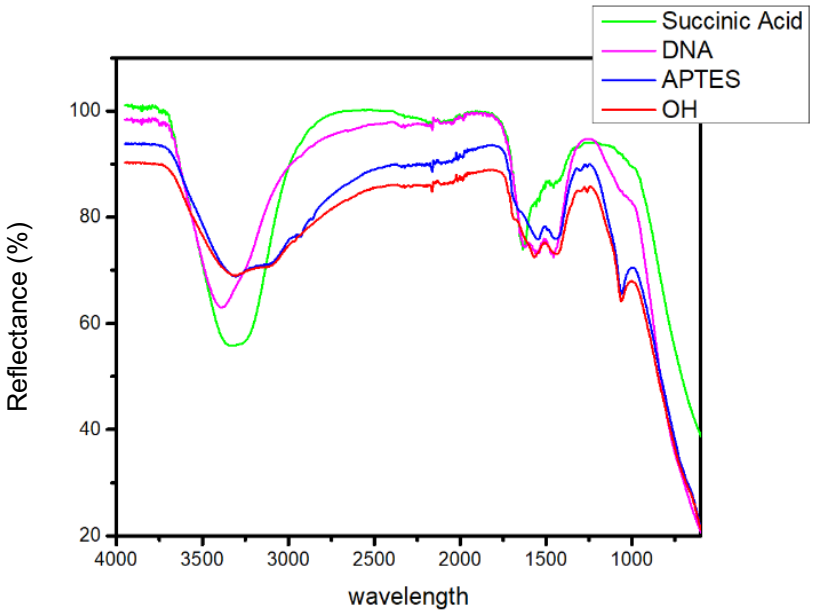

Figure 22. Reflectance spectrum comparing hydroxylated pAAO substrate (red), silanized pAAO substrate (blue), silanized pAAO substrate treated with succinic acid (green) and pAAO substrate after being activated with EDC/NHS and incubated with ssDNA capture probe (pink).

Near the value 1444, 1500 and 2000 are peaks which corresponds to cytosine, thymine and guanine bases respectively. These peaks are representative of successful DNA conjugation [30].

3.2 Sensing results

Using porous substrates as sensing platform enables the detection of analytes based on a sensing mechanism that relies on measuring the partial blockage of pores upon analyte recognition. When DNA hybridization occurs, the pores experience a partial blockage that can be measured electrochemically by introducing a redox species into the solution. The diffusion of this redox species is impeded due to a combination of steric effects (hybridization of complementary ssDNA with immobilized ssDNA capture probe) and electrostatic effects (introduction of additional negative charges by the target ssDNA, causing repulsion of ferrocyanide/ferricyanide ions diffusing through the pores).

For the experimental setup, various concentrations of target DNA ranging from 0.1 pM to 1000 pM prepared in 0.1 M PBS buffer at pH 7.4, were incubated on the sensors. To ensure the reliability of the sensing platform prepared with pAOO membranes, three sensors and three controls were employed for reproducibility assessment. For the electrochemical sensing experiments, first the C-SPEs were activated. Next, ssDNA capture probe-modified pAAO membranes featuring an average pore diameter of 40 nm were placed on top of these electrodes (Figure 23(a)) and they were clamped in an in-house custom built teflon cell with the possibility to use external reference and auxiliary electrodes (Figure 23(b)).

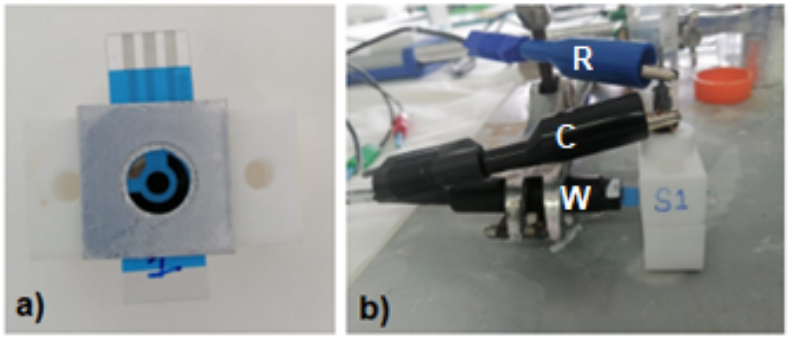

Figure 23.: a) Assembly of the fabricated membranes on the C-SPE, b) cell containing the electrode and the fabricated membrane. The electrochemical cell was comprised of a working electrode (W), a reference electrode (R) and a counter electrode (C) that closes the electrical circuit.

The electrochemical response using CV, EIS and SWV was recorded for all the membrane-modified sensors in a 2 mM ferrocyanide and 2 mM ferricyanide solution prepared in PBS. Measurements were repeated till stability was achieved prior to incubating the target DNA.

The obtained results were compared to the response from control cells prepared with a ssDNA capture probe with random oligonucleotide sequence that is not expected to hybridize to the target DNA. The EIS data were fitted into Randle's circuit, allowing the determination of the charge transfer resistance (Rct) for each sensor and control at all concentrations. As the concentration of the target DNA increased, hindrance to the diffusion of the redox species also increased. Consequently, the Rct was expected to increase (as depicted in Graph 3(a)). Additionally, in SWV, it was anticipated that the peak current would decrease for the sensors due to the hindered diffusion caused by the increasing concentrations of target DNA. Conversely, for the control cells, both the Rct and peak current values were expected to remain stable, as no DNA hybridization was anticipated (as shown in Graph 3(b)).

The obtained results were fitted into linear equations.
For EIS measurements, the following equations were derived:
Sensors: $y = 0.1083x + 1.5264$, $R^2 = 0.9771$
Controls: $y = 0.0384x + 0.4721$, $R^2 = 0.9246$

For SWV measurements, the following equations were obtained:
Sensors: $y = -0.0453x – 0.6867$, $R^2 = 0.9641$
Controls: $y = -0.0274x – 0.3158$, $R^2 = 0.9313$

These linear equations in the form of $y = mx + n$, include m as the slope of the linear fit which corresponds to the sensitivity of the sensors. Further, the theoretical limit of detection (LOD) for the sensors were calculated. The LOD of an analytical procedure refers to the minimum amount of analyte in a sample that can be detected, although not necessarily measured accurately. One method for determining the LOD involves using the mean of the blank (measurements in buffer) plus three times the standard deviation of the blank [31]. Using this formula for EIS data, the LOD was calculated to be 0.01 pM.

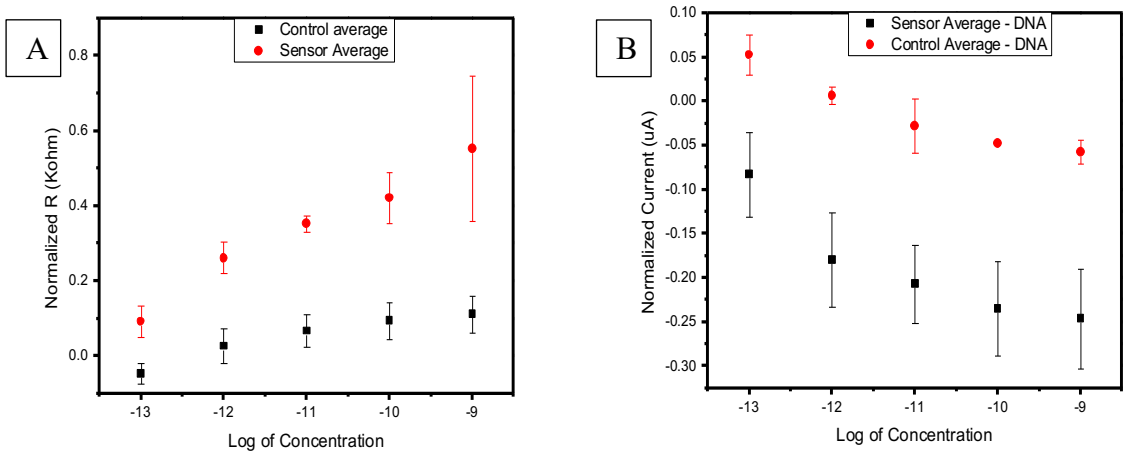

Graph 3. Calibration curves obtained from the EIS (A) and SWV (B) measurements performed with three controls and three sensors prepared by assembling the fabricated pAAO membranes on C-SPEs, upon their incubation into increasing concentrations of target ssDNA, complementary to the ssDNA immobilized on the sensors.

3.1.3 Regeneration Study

The sensors were initially employed for DNA sensing, and subsequently, a regeneration process was implemented to restore the sensor surface for further use. The regeneration process involved treating the sensors with 4 M urea solution for a duration of 1 hour. Urea is known to disrupt non-covalent interactions, which aids in the removal of hybridized DNA molecules from the sensor surface. Following the urea treatment, the sensors were thoroughly washed with copious amounts of water to ensure complete removal of urea and any remaining DNA residues. This regeneration step was crucial in preparing the sensor surface for subsequent sensing cycles. The regenerated sensors were then subjected to the highest concentration of DNA to evaluate their response. Initially, the sensors exhibited satisfactory performance during the first sensing cycle. However, as the experiments progressed, the pAAO membranes displayed signs of degradation, potentially impacting the overall sensor performance. Graph 4 displays the average normalized Rct of 2 sensors after incubating the sensor with a 1 nm solution of target DNA and subsequently the normalized Rct after 3 cycles of regeneration. The sensors were re-incubated with 1nm of target DNA for 30 minutes at room temperature after each regeneration cycle.

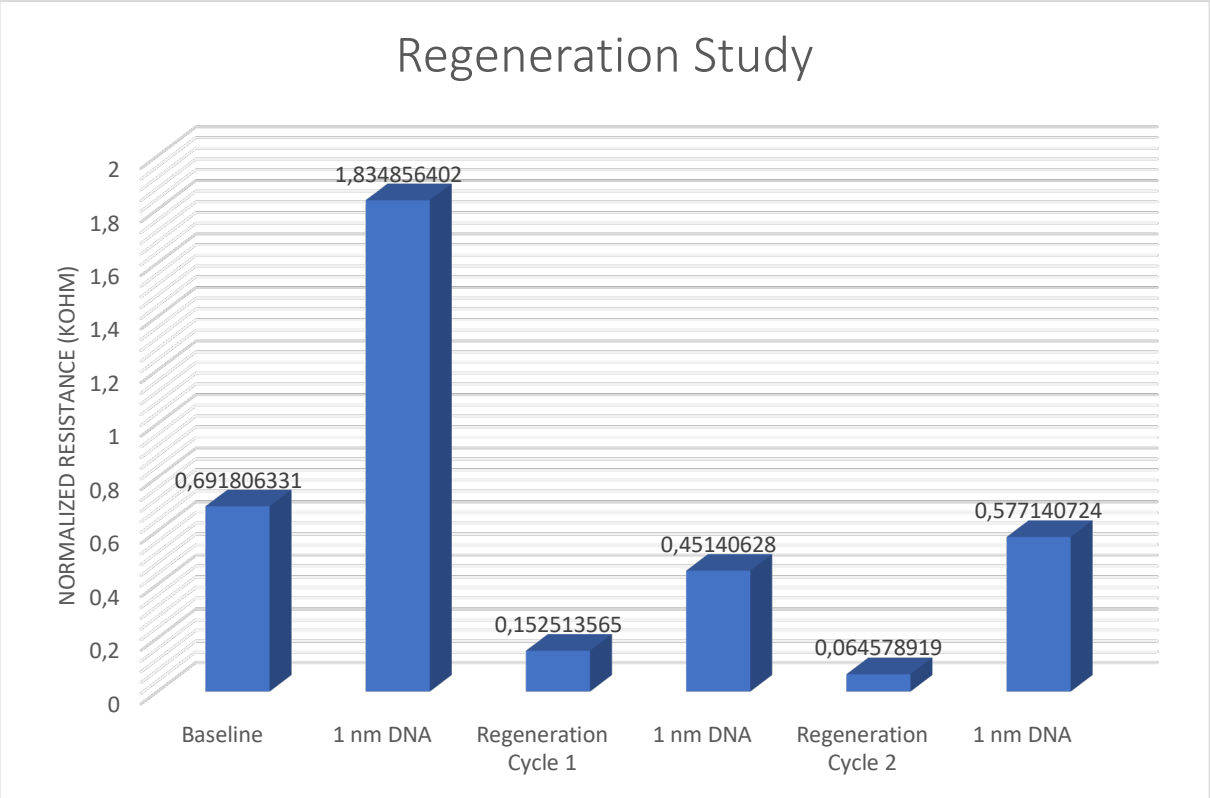

Graph 4: Regeneration study displaying the average of normalized Rct for 2 sensors before and after regeneration and subsequent DNA hybridization for 3 cycles.

4 Conclusions and future work

In conclusion, our work focused on the development of an electrochemical sensor with the required sensitivity to detect a specific miRNA, which serves as a biomarker for the early detection of lung cancer. Initial studies were conducted using a model DNA sequence as the target analyte, considering its cost-effectiveness and stability, making it suitable for optimization purposes. To achieve a highly sensitive sensor, we designed the platform to incorporate a sensing mechanism based on pore blockage. This choice was made based on previous reports suggesting that sensors utilizing pore blockage demonstrate improved sensitivity compared to those relying on flat electrodes. Through our experiments using EIS and SWV as detection techniques, results showed that Rct values obtained from EIS measurements increased as the concentration of the target DNA increased, while in SWV, the oxidation peak current decreased with increasing concentrations of the target DNA. Sensing results showed good reproducibility, high sensitivity and an LOD of 0.01 pM, which is below the expected range of concentrations of both free miRNAs in blood, and in exosomal contents.

In future work, our focus will shift towards detecting miRNA using these developed sensors and comparing their response against the DNA sensors. This investigation will allow us to evaluate the sensors' capability to specifically detect miRNA, which is a critical biomarker for lung cancer at its early stages. By comparing the response of the miRNA sensors to the DNA sensors, we can assess the effectiveness and selectivity of our sensing platform. Furthermore, we plan to explore additional optimization strategies to enhance the sensitivity and reliability of the sensing platform. This could involve modifications to the pore structure, surface functionalization, or

integration of amplification strategies to further improve the LODs and overall performance. Overall, our findings lay a strong foundation for the development of a sensitive miRNA sensor for early stage lung cancer detection, with the potential to contribute to improved diagnostic approaches and ultimately save lives through early intervention.

5 References

[1] '94865.pdf'. Accessed: Jun. 08, 2023. [Online]. Available: https://digibug.ugr.es/bitstream/handle/10481/82094/94865.pdf?sequence=4&isAllowed=y
[2] M. A. Varela, R. B. Moreno, R. L. Jime, and M. G. C. Díaz, 'POTENCIAL USO BIOMARCADOR DE LOS RETROTRANSPOSONES EN EL ADENOCARCINOMA DE PULMÓN'.
[3] 'Cáncer de pulmón microcítico | Roche Pacientes'. https://rochepacientes.es/cancer/pulmon/que-es-cancer-pulmon-microcitico.html (accessed Jun. 08, 2023).
[4] 'MRM_TESIS.pdf'. Accessed: Jun. 08, 2023. [Online]. Available: https://www.tesisenred.net/bitstream/handle/10803/401865/MRM_TESIS.pdf?sequence=1&isAllowed=y
[5] E. J. Ostrin, D. Sidransky, A. Spira, and S. M. Hanash, 'Biomarkers for Lung Cancer Screening and Detection', *Cancer Epidemiol. Biomarkers Prev.*, vol. 29, no. 12, pp. 2411–2415, Dec. 2020, doi: 10.1158/1055-9965.EPI-20-0865.
[6] C. Brambilla *et al.*, 'Early detection of lung cancer: role of biomarkers', *Eur. Respir. J.*, vol. 21, no. 39 suppl, pp. 36s–44s, Jan. 2003, doi: 10.1183/09031936.02.00062002.
[7] P. J. Mazzone *et al.*, 'Evaluating Molecular Biomarkers for the Early Detection of Lung Cancer: When Is a Biomarker Ready for Clinical Use? An Official American Thoracic Society Policy Statement', *Am. J. Respir. Crit. Care Med.*, vol. 196, no. 7, pp. e15–e29, Oct. 2017, doi: 10.1164/rccm.201708-1678ST.
[8] 'How to Detect Lung Cancer | Lung Cancer Tests'. https://www.cancer.org/cancer/types/lung-cancer/detection-diagnosis-staging/how-diagnosed.html (accessed Jun. 12, 2023).
[9] G. Rajeev, B. Prieto Simon, L. F. Marsal, and N. H. Voelcker, 'Advances in Nanoporous Anodic Alumina-Based Biosensors to Detect Biomarkers of Clinical Significance: A Review', *Adv. Healthc. Mater.*, vol. 7, no. 5, p. 1700904, Mar. 2018, doi: 10.1002/adhm.201700904.
[10] E. Xifre-Perez, J. Ferre-Borrull, and L. F. Marsal, 'Oligonucleotic Probes and Immunosensors Based on Nanoporous Anodic Alumina for Screening of Diseases', *Adv. Mater. Technol.*, vol. 7, no. 9, p. 2101591, 2022, doi: 10.1002/admt.202101591.
[11] 'Surface Functionalized Anodic Aluminum Oxide Membrane for Opto-Nanofluidic SARS-CoV-2 Genomic Target Detection', *Ieee Sens. J.*, vol. 21, no. 20, pp. 22645–22650, Aug. 2021, doi: 10.1109/JSEN.2021.3109022.
[12] H. Schwarzenbach, 'Methods for quantification and characterization of microRNAs in cell-free plasma/serum, normal exosomes and tumor-derived exosomes', *Transl. Cancer Res.*, vol. 7, no. Suppl 2, Mar. 2018, doi: 10.21037/tcr.2017.09.50.
[13] E. I. Yakubovich, A. G. Polischouk, and V. I. Evtushenko, 'Principles and Problems of Exosome Isolation from Biological Fluids', *Biochem. Mosc. Suppl. Ser. Membr. Cell Biol.*, vol. 16, no. 2, pp. 115–126, 2022, doi: 10.1134/S1990747822030096.
[14] S. S. Low *et al.*, 'Recent Progress in Nanomaterials Modified Electrochemical Biosensors for the Detection of MicroRNA', *Micromachines*, vol. 12, no. 11, p. 1409, Nov. 2021, doi: 10.3390/mi12111409.
[15] L. Zhang *et al.*, 'Recent Progresses in Electrochemical DNA Biosensors for MicroRNA Detection', *Phenomics*, vol. 2, no. 1, pp. 18–32, Jan. 2022, doi: 10.1007/s43657-021-00032-z.
[16] M. El Aamri, G. Yammouri, H. Mohammadi, A. Amine, and H. Korri-Youssoufi, 'Electrochemical Biosensors for Detection of MicroRNA as a Cancer Biomarker: Pros and

Cons', *Biosensors*, vol. 10, no. 11, p. 186, Nov. 2020, doi: 10.3390/bios10110186.
[17] J. H. Kim *et al.*, 'Technological advances in electrochemical biosensors for the detection of disease biomarkers', *Biomed. Eng. Lett.*, vol. 11, no. 4, pp. 309–334, Nov. 2021, doi: 10.1007/s13534-021-00204-w.
[18] S. Cai *et al.*, 'Single-molecule amplification-free multiplexed detection of circulating microRNA cancer biomarkers from serum', *Nat. Commun.*, vol. 12, no. 1, Art. no. 1, Jun. 2021, doi: 10.1038/s41467-021-23497-y.
[19] A. Santos, L. Vojkuvka, J. Pallarés, J. Ferré-Borrull, and L. F. Marsal, 'In situ electrochemical dissolution of the oxide barrier layer of porous anodic alumina fabricated by hard anodization', *J. Electroanal. Chem.*, vol. 632, no. 1–2, pp. 139–142, Jul. 2009, doi: 10.1016/j.jelechem.2009.04.008.
[20] A. Santos Alejandro, 'Structural engineering of nanoporous anodic alumina and applications', Ph.D. Thesis, Universitat Rovira i Virgili, 2010. Accessed: Jun. 08, 2023. [Online]. Available: https://www.tdx.cat/handle/10803/8480
[21] 'What is Electropolishing? How Does Electropolishing Work?', *Best Technology*. https://www.besttechnologyinc.com/electropolishing-equipment/how-does-electropolishing-work/ (accessed May 08, 2023).
[22] P. Tyagi, T. Goulet, C. Riso, K. Klein, and F. Garcia-Moreno, *ELECTROPOLISHING OF ADDITIVELY MANUFACTURED HIGH CARBON GRADE 316 STAINLESS STEEL*. 2018. doi: 10.31224/osf.io/5dn49.
[23] A. Casasanero Meléndez, 'Nanoestructuración electroquímica de óxido de aluminio por medio de anodización y electropulido', Feb. 2013, Accessed: Jun. 08, 2023. [Online]. Available: http://tesis.ipn.mx/xmlui/handle/123456789/11235
[24] 'El anodizado de Aluminio', *AFV Inicia Aluminio Anodizado*. https://www.afvinicia.com/el-anodizado-de-aluminio/ (accessed Jun. 08, 2023).
[25] G. Sulka, L. Zaraska, and W. Stępniowski, 'Anodic porous alumina as a template for nanofabrication', in *Encyclopedia of Nanoscience and Nanotechnology*, 2011, pp. 261–349.
[26] Y. Patel, G. Janusas, A. Palevicius, and A. Vilkauskas, 'Development of Nanoporous AAO Membrane for Nano Filtration Using the Acoustophoresis Method', *Sensors*, vol. 20, no. 14, Art. no. 14, Jan. 2020, doi: 10.3390/s20143833.
[27] C. Y. Han, G. A. Willing, Z. Xiao, and H. H. Wang, 'Control of the Anodic Aluminum Oxide Barrier Layer Opening Process by Wet Chemical Etching', *Langmuir*, vol. 23, no. 3, pp. 1564–1568, Jan. 2007, doi: 10.1021/la060190c.
[28] A. Shiohara *et al.*, 'SARS-CoV-2 Virus Detection Via a Polymeric Nanochannel-Based Electrochemical Biosensor', *Small*, vol. n/a, no. n/a, p. 2205281, doi: 10.1002/smll.202205281.
[29] P. Hampitak *et al.*, 'A Point-of-Care Immunosensor Based on a Quartz Crystal Microbalance with Graphene Biointerface for Antibody Assay', *ACS Sens.*, vol. 5, no. 11, pp. 3520–3532, Nov. 2020, doi: 10.1021/acssensors.0c01641.
[30] V. Reddy *et al.*, 'Electrochemical Detection of Single Nucleotide Polymorphism in Short DNA Sequences Related To Cattle Fatty Acid Binding Protein 4 Gene', *Int J Electrochem Sci*, vol. 7, 2012.
[31] 'Limit of Blank, Limit of Detection and Limit of Quantitation - PMC'. https://www.ncbi.nlm.nih.gov/pmc/articles/PMC2556583/ (accessed Jun. 13, 2023).